# Vacancies in graphene: Dirac physics and fractional vacuum charges

Omrie Ovdat, Yaroslav Don, and Eric Akkermans*
*Department of Physics, Technion – Israel Institute of Technology, Haifa 3200003, Israel*

(Received 13 September 2018; revised 12 March 2019; accepted 14 July 2020; published 7 August 2020)

The study of vacancies in graphene is a topic of growing interest. A single vacancy induces a localized stable charge of order unity interacting with other charges of the conductor through an unscreened Coulomb potential. It also breaks the symmetry between the two triangular graphene sublattices hence inducing zero energy states at the Dirac points. Here we show the fractional and pseudoscalar nature of this vacancy charge. A continuous Dirac model is presented which relates zero modes to vacuum fractional charge and to a parity anomaly. This relation constitutes an index theorem and is achieved by using particular chiral boundary conditions, which map the vacancy problem onto edge state physics. Vacancies in graphene thus allow us to realize prominent features of $2+1$ quantum electrodynamics but without coupling to a gauge field. This essential difference makes vacancy physics relatively easy to implement and an interesting playground for topological state switching.

DOI: 10.1103/PhysRevB.102.075109

## I. INTRODUCTION AND STATEMENT OF RESULTS

Graphene has a remarkable low energy spectrum described by an effective Dirac model, whose interest resides in its ability to account for a wealth of fundamental aspects specific to massless Dirac fermions. Vacancies [1–18], obtained by removing neutral carbon atoms, have important consequences for the physics of graphene: (i) Zero energy modes. In the presence of $N_A + N_B$ vacancies, where $N_A$ ($N_B$) is the number of vacancies corresponding to sublattice $T_A$ ($T_B$), the tight-binding Hamiltonian has $|N_A - N_B|$ zero energy eigenvalues with vanishing wave function on the minority sublattice [1–6]. (ii) Charge. Density functional theory calculations [7] show that when a carbon atom is removed, the induced electronic rearrangement leads to a lower energy configuration and to an overall local electric charge in the ground state. In addition, tunneling and Landau level spectroscopy [6] provide experimental support for the existence of this local charge and show, with very good agreement, an energy spectrum corresponding to an unscreened $V \sim -1/r$ Coulomb potential (see Fig. 1). (iii) Symmetry breaking. For $N_A \neq N_B$, sublattice symmetry is broken and so is parity in the continuum limit. For a single vacancy, the degeneracy lifting between the two lowest angular momentum channels $j = \pm 1/2$, a clear indication of parity symmetry breaking, has been indeed observed (see Fig. 1).

In this paper, we present a continuous Dirac model of graphene, valid at low energy and applicable to an arbitrary configuration of isolated vacancies, which accounts for the above features and shows their direct relation. The localized, fractional, and pseudoscalar nature of the vacancy charge is a consequence of the asymmetry between positive and negative parts of the spectrum as expressed by the occurrence of zero energy modes. This fractional charge does not display Friedel-like density oscillations and essentially differs from the screening resulting from the insertion of external charge defects [19–25]. The vacuum charge density and its corresponding charge are obtained by solving the scattering problem of massless Dirac fermions by one vacancy while imposing on their wave function a new type of 'chiral' boundary conditions. This choice unveils the topological nature of the charge and its relation to zero modes under the form of an index theorem. We emphasize how the phenomena of a charged vacancy presented here, realizes the physics of fermion number fractionalization [26–42] with the topological content of the magnetic flux $\Phi$ now replaced by vacancies with properly chosen boundary conditions such that

$$N_A - N_B \leftrightarrow \Phi. \tag{1}$$

## II. DIRAC MODEL

In graphene, carbon atoms condense into a planar honeycomb bipartite lattice built from two triangular sublattices $T_A$ and $T_B$. The Bravais lattice with a two-atom unit cell and its reciprocal are triangular and the hexagonal Brillouin zone has two inequivalent crystallographic Dirac points $K$ and $K'$. Around each of them, the low energy excitation spectrum is conveniently described by noninteracting and in-plane massless Dirac fermions with the effective continuous Hamiltonian,

$$H = -i\,\boldsymbol{\sigma}\cdot\boldsymbol{\nabla} = \begin{pmatrix} 0 & D \\ D^\dagger & 0 \end{pmatrix} \tag{2}$$

($\hbar = v_F = 1$), $D = -i\partial_x - \partial_y = e^{-i\theta}(-i\partial_r - \frac{1}{r}\partial_\theta)$ and $\boldsymbol{\sigma} = (\sigma_x, \sigma_y)$. This description was shown to be valid at low energies even in the presence of electron-electron interactions up to logarithmic corrections to the Fermi velocity [43,44] (see Supplemental Material [45]). The operators $D$ and $D^\dagger$ are defined on the direct sum $\mathcal{H}_A \oplus \mathcal{H}_B$ of Hilbert spaces associated to $T_A$ and $T_B$ and the corresponding quantum states are two-component spinors $\psi(\boldsymbol{r}) = (\psi^A \quad \psi^B)^T$, with $\psi^{A,B}$ being quantum amplitudes on $T_A$ and $T_B$, respectively, at

*eric@physics.technion.ac.il

 

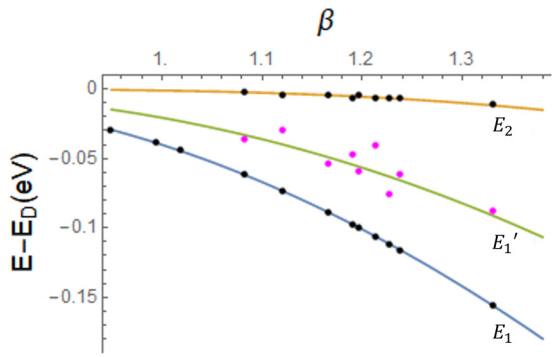


FIG. 1. Experimental observation of the massless Dirac-Coulomb spectrum in graphene with broken sublattice/parity symmetry (see Ref. [8] for more details). The continuous lines above are derived from the exact solution of the massless Dirac-Coulomb system where $\beta$ is the Coulomb strength and $E_D$ is the Dirac point. The curves $E_1, E_1', E_2$ describe quasibound states extracted from the total density of states of the $j = 1/2$ ($E_1$, $E_2$) and $j = -1/2$ ($E_1'$) total angular momentum channels. $E_1$, $E_2$, and $E_1'$ are also the lowest quasibound states appearing for the corresponding $\beta > 1/2$ values in the plot. The black and magenta dots correspond to experimental points obtained at a charged vacancy in graphene. These are obtained from tunneling conductance data measured as a function of tunneling voltage at the vacancy site. The existence of the middle branch is a clear signal for the degeneracy lifting between the two lowest angular momentum channels $j = \pm 1/2$ and thereby an indication of parity symmetry breaking.

a coarse grained position $\boldsymbol{r}$. The spectrum of $H$ spans the continuum, but positive and negative parts can be mapped one onto the other, a symmetry expressed by

$$\{H, \sigma_z\} = 0\,, \tag{3}$$

and hereafter called chiral, which is a consequence of the bipartite structure of the lattice. Moreover, the honeycomb lattice is invariant under spatial inversion $\boldsymbol{r} \mapsto -\boldsymbol{r}$ which decomposes into two mirror symmetries where parity,

$$x \mapsto x,\ y \mapsto -y, H \mapsto \sigma_x H \sigma_x, \tag{4}$$

exchanges the two sublattices $T_A$ and $T_B$.

The vacuum charge density,

$$\rho(\boldsymbol{r}) = -e \sum_{n, E_n<0} \psi_n^\dagger(\boldsymbol{r})\psi_n(\boldsymbol{r}) + e \sum_{n, E_n<0} \psi_n^\dagger(\boldsymbol{r})\psi_n(\boldsymbol{r})\Big|_{\text{free}}, \tag{5}$$

corresponds to the particle density associated with electrons filling all the negative energy states relative to the same quantity in absence of any potentials. Utilizing the completeness relation $\rho(\boldsymbol{r})$ takes the symmetric form [46,47],

$$\rho(\boldsymbol{r}) = \frac{e}{2} \sum_n \text{sgn}\,(E_n)\psi_n^\dagger(\boldsymbol{r})\psi_n(\boldsymbol{r}). \tag{6}$$

For an infinite system, the charge density $\rho(\boldsymbol{r})$ is a total divergence (see Refs. [47,48] and Supplemental Material [45]),

$$\rho(\boldsymbol{r}) = \frac{e}{2}\,\text{sgn}\,(M)\boldsymbol{\nabla}\cdot\boldsymbol{\Delta}(\boldsymbol{r}), \tag{7}$$

where the regularizing mass parameter $M \to 0$ removes the sign ambiguity in (6) in the presence of zero modes. The ambiguity associated with $E = 0$ results from the necessity to determine whether or not $E = E_F = 0$ states are occupied. The introduction of a small mass term is one way to regularize this ambiguity. The mass term shifts the zero modes to $\pm M$ which, depending on the sign, discriminates between occupying the zero modes or not. The matrix element

$$\boldsymbol{\Delta}(\boldsymbol{r}) \equiv \frac{1}{2}\langle \boldsymbol{r}|\,\text{tr}\left(\boldsymbol{\sigma}\sigma_z \frac{1}{H - i0}\right)|\boldsymbol{r}\rangle \tag{8}$$

is a two-dimensional vector and "tr" is over spinor indices.

Despite being defined over the entire energy spectrum, $\rho(\boldsymbol{r})$ turns out to be related to a quantity evaluated at the Fermi energy, a noteworthy result since (2) is merely valid close to $E = 0$. Furthermore, (7) is directly related to features of the zero-energy subspace. Its dimension, $\dim\ker D + \dim\ker D^\dagger$, obtained by counting all solutions of $D\psi_B = D^\dagger\psi_A = 0$, cannot generally be determined, but the relation,

$$\text{index}\,H = -\,\text{sgn}\,(M)\int d\boldsymbol{r}\,\boldsymbol{\nabla}\cdot\boldsymbol{\Delta}(\boldsymbol{r}), \tag{9}$$

holds for $\text{index}\,H \equiv \dim\ker D - \dim\ker D^\dagger$ [46,47]. Combining (7) and (9) leads to

$$Q \equiv \int d\boldsymbol{r}\rho(\boldsymbol{r}) = -\frac{e}{2}\,\text{index}\,H\,. \tag{10}$$

In the absence of vacancies, there are no zero modes thus index $H$ vanishes and so does the charge $Q$ and $\rho(\boldsymbol{r})$. However, this may not be the case in the presence of vacancies.

## III. SCATTERING DESCRIPTION OF SINGLE VACANCY

The removal of one carbon atom creates a vacancy, here arbitrarily assigned to be an $A$ vacancy [49]. The corresponding excitation spectrum in the continuum limit is obtained by considering scattering solutions of the Dirac Hamiltonian (2) on a plane with a puncture of radius $R$. Since $\rho(\boldsymbol{r})$ depends on the behavior at zero energy, we look for zero modes, i.e., solutions of $D\psi_B = D^\dagger\psi_A = 0$. The general solution is

$$\psi(r,\theta) \equiv \sum_{m\in\mathbb{Z}} e^{im\theta}\begin{pmatrix}\psi_m^A(r)\\ i\psi_m^B(r)e^{i\theta}\end{pmatrix} \tag{11}$$

with $\psi_m^A(r) = A_m r^m$, $\psi_m^B(r) = B_m r^{-m-1}$ and $(A_m, B_m)$ constants. Requiring $\psi(r\to\infty,\theta) = 0$, we keep harmonics $m < 0$ for $\psi_m^A(r)$ and $m \geqslant 0$ for $\psi_m^B(r)$.

### A. Chiral boundary conditions

We choose appropriate boundary conditions on the scattering potential. Local boundary conditions, e.g., Dirichlet, $\psi(\boldsymbol{r})|_{\text{vac}} = 0$ lead either to an over determination or to particle-hole pair creation (Neumann) [50]. We propose instead a new set of chiral boundary conditions,

$$\begin{aligned}\psi_m^A(r = R) &= 0, \quad m \leqslant 0,\\ \psi_m^B(r = R) &= 0, \quad m > 0,\end{aligned} \tag{12}$$

a close relative of nonlocal boundary conditions introduced in the study of index theorems for Dirac operators [51–53]. This

TABLE I. Boundary condition. Boundary conditions for an $A/B$ vacancy imposed on the radial components $\psi_m^{A,B}$. The conditions differ only for $m = 0, -1$ ($j = \pm 1/2$).

| | $A$ vacancy | | $B$ vacancy | |
|---|---|---|---|---|
| $m$ | $\psi_m^A(R)$ | $\psi_m^B(R)$ | $\psi_m^A(R)$ | $\psi_m^B(R)$ |
| $\leqslant -2$ | 0 | | 0 | |
| $-1$ | 0 | | | 0 |
| 0 | 0 | | | 0 |
| $\geqslant 1$ | | 0 | | 0 |

choice (12) preserves the chiral symmetry (3), a necessary condition to use expressions (7)–(10) and represent a perfectly reflecting barrier of probability density (Supplemental Material [45]). Implemented on the power law wave function (11), conditions (12) uniquely lead to a single zero mode

$$\psi(\boldsymbol{r}) \equiv \begin{pmatrix} 0 \\ iB_0 e^{i\theta}/r \end{pmatrix} \tag{13}$$

by projecting onto the $m = 0$ subspace for $\psi_m^B(r)$ and having $\psi_m^A \equiv 0$. It is worth noting that this eigenfunction reproduces the tight binding result [3] justified by the absence of any characteristic scale. This zero mode is quasibound, that is, decaying but non-normalizable and thus appears as a pronounced peak in the density of states at the Fermi energy. An analogous choice of boundary conditions for a $B$ vacancy, presented in Table I, leads to the single zero mode $\psi(\boldsymbol{r}) \equiv (A_{-1}/r \quad 0)^T$ [54].

### B. Parity symmetry breaking

As required by sublattice symmetry breaking, chiral boundary conditions (12) do not preserve parity which in the continuous limit, corresponds to $m \leftrightarrow -m-1$, $\psi_m^A \leftrightarrow -\psi_{-m-1}^B$ and $\psi_m^B \leftrightarrow \psi_{-m-1}^A$. Indeed, unlike the parity preserving choice,

$$\begin{aligned} \psi_m^A(r=R) &= 0, \quad m > 0, \\ \psi_m^B(r=R) &= 0, \quad m \leqslant 0, \end{aligned} \tag{14}$$

under conditions (12), the $m = 0$ solution $\psi_0^B(r) = ie^{i\theta}/r$ does not transform into the vanishing $m = -1$ solution $\psi_{-1}^A(r)$. We thus conclude that the presence of a vacancy necessarily breaks parity and removes the $j = \pm 1/2$ degeneracy, where $j \equiv m + 1/2$. This point is particularly relevant in light of recent observation of $j = \pm 1/2$ degeneracy breaking by STM spectroscopy at a vacancy site [8] (Fig. 1).

### C. Results—Single vacancy

To relate the existence of the zero mode to a finite vacuum charge density as given in (9)–(10), we must directly calculate the index in (9). To that aim, we use the regularized expression [48],

$$\operatorname{index} H = \lim_{z\to 0} \operatorname{Tr}\left(\frac{z}{H^B + z} - \frac{z}{H^A + z}\right), \tag{15}$$

where $H^B \equiv D^\dagger D$ and $H^A \equiv DD^\dagger$. The "Tr" operation here is over all states. Hereafter we take $\operatorname{sign} M \equiv 1$ in (9), thus

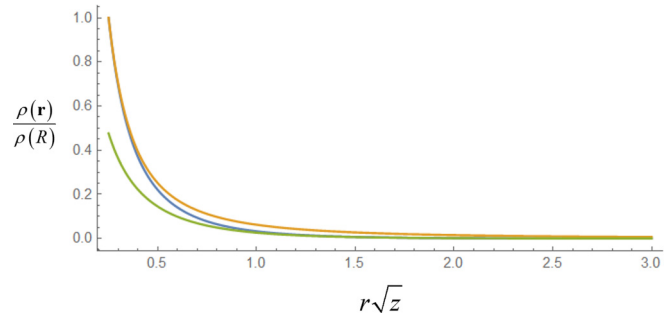


FIG. 2. Single vacancy charge density. Blue: Characteristic behavior of $\rho(\boldsymbol{r})/\rho(R)$ in (18) as a function of $x \equiv r\sqrt{z}$ with $y \equiv R\sqrt{z} = 0.25$. Orange: The function $y^2/x^2$. Green: The function $\pi y^2 e^{-2x}/x$.

arbitrarily fixing the sign of the charge for an $A$ vacancy. Extending chiral boundary conditions (12) to nonzero energy scattering states involved in (15) shows how the angular momentum contributions cancel out except for $j = \pm 1/2 \leftrightarrow m = -1, 0$. A thorough calculation (Supplemental Material [45]) yields

$$\operatorname{index} H = -\frac{1}{2\pi R} \lim_{z\to 0} \int d\boldsymbol{r}\, \nabla \cdot \left( \frac{K_0(\sqrt{z}r) K_1(\sqrt{z}r)}{K_0(\sqrt{z}R) K_1(\sqrt{z}R)} \hat{r} \right), \tag{16}$$

where $K_n(x)$ are the modified Bessel functions of the second kind. Integrating (16) in the region $R < r < \infty$, $0 < \theta < 2\pi$ and inserting into (10) gives

$$Q = -\frac{e}{2} \operatorname{index} H = -\frac{e}{2} \cdot (\lim_{z\to 0} 1) = -\frac{e}{2} \cdot 1. \tag{17}$$

The charge density $\rho(\boldsymbol{r})$ can be read off the integrand [55] in (16)

$$\rho(\boldsymbol{r}) = -\frac{e}{4\pi R} \nabla \cdot \left( \frac{K_0(\sqrt{z}r) K_1(\sqrt{z}r)}{K_0(\sqrt{z}R) K_1(\sqrt{z}R)} \hat{r} \right). \tag{18}$$

In the limit of a pointlike vacancy, $R \to 0$, $\rho(\boldsymbol{r})$ vanishes $\forall r \neq 0$. Since $\int d\boldsymbol{r}\, \rho(\boldsymbol{r}) = -e/2$, independent of $R$, $\rho(\boldsymbol{r})$ can be represented by the $\delta$-function distribution

$$\lim_{R\to 0} \rho(\boldsymbol{r}) = -\frac{1}{2\pi} \nabla \cdot \left( \frac{e/2}{r} \hat{r} \right). \tag{19}$$

For finite $R$, $\rho(\boldsymbol{r})$ can be approximated from (18) with an arbitrarily small finite value of $z$ acting as an IR cutoff. For $r\sqrt{z} \gg 1$, $\rho(r)/\rho(R) \approx \exp(-2\sqrt{z}r)$ and for $r\sqrt{z} \ll 1$, $R\sqrt{z} \ll 1$, $\rho(r)/\rho(R) \approx R^2/r^2$. Thus, the charge density decays close to the vacancy as $\sim 1/r^2$ and decays exponentially, far from the vacancy (see Fig. 2).

The resulting charge density $\rho(\boldsymbol{r})$ is thus a total divergence with a fractional vacuum charge $Q = -e/2$, localized at the boundary of the vacancy (Figs. 2 and 3). In the simplest approximation the corresponding potential, induced by electron interaction, is Coulomb-like, i.e., decays as $1/r$. The same conclusions apply to a $B$ vacancy but with an opposite sign of the charge (Supplemental Material [45]). This sign flip $Q \to -Q$ in the exchange $T_A \leftrightarrow T_B$ points to the pseudoscalar nature of the vacuum charge. Hence a nonzero $Q$ provides a clear signal for the breaking of parity symmetry of the ground

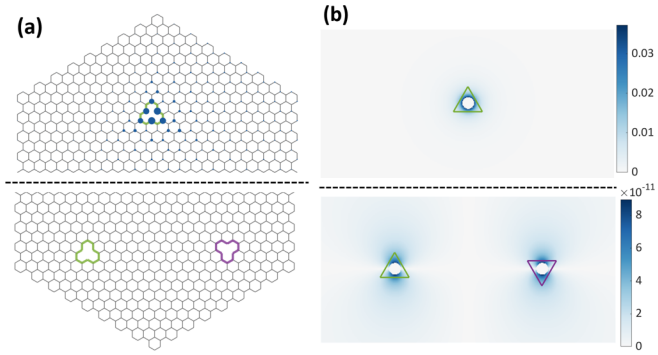


FIG. 3. Charge of vacancy configurations. Top: Single $A$ vacancy ($N_A = 1, N_B = 0$). There is one zero mode, index $H = |N_A - N_B| = 1$ and a finite fractional charge $Q = e/2$. Bottom: $N_A = N_B = 1$. Adding a $B$ vacancy, the zero mode disappears, index $H = |N_A - N_B| = 0$, and so does the fractional charge on both vacancy locations represented for visual aid, by the green ($A$-vacancy) and purple ($B$-vacancy) outlines. (a) Tight-binding calculation of the spatial charge density $|\rho(\boldsymbol{r})|$ obtained from definition Eq. (6) and depicted by the blue spots. The total charge in a two lattice spacing radius is $Q \approx 10^{-1}$ (in units of $e/2$) for the single vacancy (top) and $Q_\triangle, Q_\triangledown \approx 10^{-8}$ for $N_A = N_B = 1$ (bottom). A small positive mass term $M \approx +10^{-9}$ has been used together with armchair boundary conditions which suppress charge accumulation on the boundary (Supplemental Material [45]). (b) Continuous Dirac model calculation of the spatial charge density $|\rho(\boldsymbol{r})|$ for the same situations as in (a). These results are obtained using low energy scattering theory (Supplemental Material [45]). Note the different scales displayed on the right color code.

state and the lifting of the $j = \pm 1/2$ degeneracy. Including spin degeneracy, the overall "fractional charge" is $2 \times Q = \pm e$.

It is interesting to further understand the origin of this finite charge. The creation of a vacancy leads to an asymmetry between positive and negative energy states. An ill-defined albeit suggestive way to visualize it is offered by the spatial integral of (6) which together with (10) gives

$$Q = \frac{e}{2}\left(\sum_{E_n>0} 1 - \sum_{E_n<0} 1\right) = -\frac{e}{2}\,\mathrm{index}\,H\,. \tag{20}$$

This "spectral asymmetry," of topological origin [51], eventually amounts to a counting of zero modes only.

All together, the fractional pseudoscalar charge, the resulting Coulomb-like potential [56] and the lifting of the $j = \pm 1/2$ degeneracy provide a comprehensive explanation to the observation of a vacancy charge and parity breaking obtained by STM measurements at a vacancy location in graphene [8]. Note that the charge density (19) does not display otherwise expected Friedel-like oscillations for the screening of a scalar charge. These findings thus constitute an original example of a nonzero index in an open space, independent of the existence of an underlying gauge field (above one spatial dimension).

## IV. MULTIPLE VACANCIES

We now generalize the previous results to arbitrary configurations of a finite number of isolated vacancies. As in the single vacancy case, this description assumes noninteracting electrons, corresponding to the Dirac and tight-binding model of graphene. We discuss the validity of the associated multivacancy features in the discussion section.

The zero mode wave functions are now difficult to obtain primarily due to multiple scattering between vacancies and the lack of rotational symmetry. Since the size of each vacancy is the lattice spacing, we assume constant wave function along the boundary of each vacancy making them pointlike scatterers [57]. Starting from the zero mode eigenfunctions,

$$\psi_\blacktriangle(z) = \frac{1}{z^* - z_A^*}\begin{pmatrix}0\\1\end{pmatrix}, \quad \psi_\blacktriangledown(z) = \frac{1}{z - z_B}\begin{pmatrix}1\\0\end{pmatrix} \tag{21}$$

established for a single $A$ or $B$ vacancy located in $z_{A,B}$, $z \equiv x + iy$, we propose the ansatz,

$$\psi_N(z) = \begin{pmatrix}0\\1\end{pmatrix}\sum_{k=1}^{N_A}\frac{q_{kA}}{z^* - z_{kA}^*} + \begin{pmatrix}1\\0\end{pmatrix}\sum_{k=1}^{N_B}\frac{q_{kB}}{z - z_{kB}} \tag{22}$$

for a configuration of $N = N_A + N_B$ vacancies located in $z_{kA}$ and $z_{kB}$. This spinor wave function $\psi_N \equiv (\psi_N^A \quad \psi_N^B)^T$ reproduces all the single vacancy features previously obtained by means of chiral boundary conditions (12), provided we require $\psi_N^A(z_{kA}) = \psi_N^B(z_{kB}) = 0$. The resulting constraints on the parameters $q_{kA,kB}$ take the matrix form,

$$M\boldsymbol{q}_B = 0, \quad M^\dagger \boldsymbol{q}_A = 0, \tag{23}$$

where $M_{ij} = (z_{iA} - z_{jB})^{-1}$ is a $N_A \times N_B$ Cauchy matrix of full rank $\forall z_{iA}, z_{jB}$ [58]. Assuming, without loss of generality, that $N_A \geqslant N_B$, then $\mathrm{rank}\,M = \mathrm{rank}\,M^\dagger = N_B$ and the solution of $M\boldsymbol{q}_B = 0$ becomes the trivial one $\boldsymbol{q}_B = 0$, while $M^\dagger \boldsymbol{q}_A = 0$ has $N_A - N_B$ independent solutions, i.e., $|N_A - N_B|$ zero modes for arbitrary $N_A, N_B$. As required, this result coincides with the number of zero modes proven to exist in any vacancy filled bipartite lattice [1–5]. Moreover, for $N_A \geqslant N_B$, all the zero modes fulfill $\psi_N^A \equiv 0$ and $D\psi_N^B = 0$, thus, for a multivacancy configuration, index = # of zero modes $= N_A - N_B$. Utilizing scattering theory, we additionally obtained a closed form expression for $\rho(\boldsymbol{r})$ as given in (7) for a general multivacancy configuration (see Supplemental Material [45]).

We now dwell on cases which illustrate the underlying features of many-vacancy configurations. In these cases we illustrate the correspondence of our Dirac model with tight-binding numerics. Starting from a single $A$ vacancy ($N_A = 1$) (Fig. 3). A zero mode appears associated to index $H = N_A = 1$, together with a vacuum charge $Q = -(1/2)e$ localized at the vacancy site and a broken parity symmetry. Adding a $B$ vacancy (Fig. 3) implies index $H = |N_A - N_B| = 0$ so that the charge vanishes at each vacancy location and parity symmetry is restored.

Adding yet another $A$ vacancy changes the situation since index $H = |N_A - N_B| = 1$ and parity symmetry is again broken. Each $A$ vacancy now holds a finite charge $Q_\blacktriangle$ smaller than $(1/2)e$ which depends on the exact spatial configuration. The $B$ vacancy carries no charge, $Q_\triangledown = 0$, a direct consequence of the vanishing of $\boldsymbol{q}_B$ in (23). These results, displayed in Fig. 4, have an attractive generalization. Consider a $N_A - N_B = 1$ configuration where all the $A$ vacancies are charged ($Q_\blacktriangle$) and the $B$ vacancies necessarily uncharged ($Q_\triangledown$). Adding

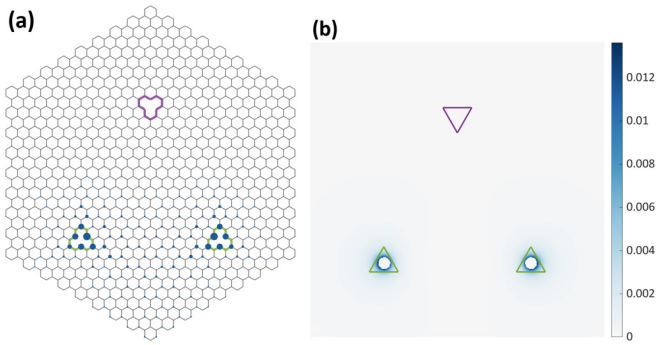


FIG. 4. Configuration of three vacancies $N_A = 2, N_B = 1$. There is one zero mode, index $H = |N_A - N_B| = 1$, so that the two $A$ vacancies (green upward outline) have a finite and equal charge $Q_▲$ in this symmetric configuration and the $B$ vacancy (purple downward outline) is not charged $Q_▽ = 0$. (a) Tight-binding calculation of the spatial charge density $|\rho(\boldsymbol{r})|$ obtained from definition Eq. (6) and depicted by the blue spots. The total charge is $Q_▲ \approx 10^{-1}$ (in units of $e/2$) and $Q_▽ \approx 10^{-4}$ on each $A, B$ vacancy, respectively. A small positive mass term $M \approx +10^{-9}$ has been used together with armchair boundary conditions which suppress charge accumulation on the boundary (Supplemental Material [45]). (b) Continuous Dirac model calculation of the spatial charge density $|\rho(\boldsymbol{r})|$ for the same situation as in (a). These results are obtained using low energy scattering theory (Supplemental Material [45]). The homogeneous purple region around the $A$ vacancies is $\approx 10^{-5}$.

a $B$ vacancy wherever in the plane markedly changes this picture by switching off all the charges in the plane $(Q_△, Q_▽)$. This feature can be viewed as a topological state switch, where the creation of one remote vacancy of the right kind switches off, at once, all the finite charges $Q_▲$ on the graphene lattice. This effect is independent of the relative position of the vacancies and results only from the vanishing of the overall index.

## V. DISCUSSION

The physics of a charged vacancy presented here bears essential similarities with $2+1$ quantum electrodynamics (QED), such as fermion number fractionalization and parity anomaly [26–42]. In the latter case, a dynamical external gauge field induces zero modes of massless planar fermions and vacuum charge with abnormal parity. The index of the corresponding Dirac operator follows (10) and acquires nonzero values proportional to the strength of the gauge field. Hence, the present results provide, for graphene, a measurable realization of these QED effects with the topological content of the gauge field now replaced by vacancies with properly chosen boundary conditions. Furthermore, our findings display a coherent description of existing measurements [6,8] and provide additional predictions that can be tested with an appropriate experimental control on multivacancy configurations. Several aspects of these features may not be realized in an experimental setup. Due to noise and interactions vacancies will only be correlated up to some finite screening length. Within this regime, interactions may also result in a broadening and delocalizing of charge around the vacancies especially if these are tightly packed. It would be interesting to study the extent of this effect in the framework of an interacting model such as the Hubbard model.

Including spin degrees of freedom in the Dirac picture and connecting with Lieb's theorem [2] may enrich the picture presented here by associating to a vacancy the quantum dynamics of a localized vacuum spin which is proportional to the Dirac index. Possible connections to recent observations of vacancy magnetic moments [11–15] should be investigated together with a generalization to other bipartite lattices and to nonisolated vacancies.

## ACKNOWLEDGMENT

This work was supported by the Israel Science Foundation Grant No. 924/09.

[1] B. Sutherland, Phys. Rev. B **34**, 5208 (1986).
[2] E. H. Lieb, Phys. Rev. Lett. **62**, 1201 (1989).
[3] V. M. Pereira, F. Guinea, J. M. B. Lopes dos Santos, N. M. R. Peres, and A. H. Castro Neto, Phys. Rev. Lett. **96**, 036801 (2006).
[4] V. M. Pereira, J. M. B. Lopes dos Santos, and A. H. Castro Neto, Phys. Rev. B **77**, 115109 (2008).
[5] B. R. K. Nanda, M. Sherafati, Z. S. Popović, and S. Satpathy, New J. Phys. **14**, 083004 (2012).
[6] J. Mao, Y. Jiang, D. Moldovan, G. Li, K. Watanabe, T. Taniguchi, M. R. Masir, F. M. Peeters, and E. Y. Andrei, Nat. Phys. **12**, 545 (2016).
[7] Y. Liu, M. Weinert, and L. Li, Nanotechnology **26**, 035702 (2015).
[8] O. Ovdat, J. Mao, Y. Jiang, E. Y. Andrei, and E. Akkermans, Nat. Commun. **8**, 507 (2017).
[9] M. Inui, S. A. Trugman, and E. Abrahams, Phys. Rev. B **49**, 3190 (1994).
[10] J. J. Palacios, J. Fernández-Rossier, and L. Brey, Phys. Rev. B **77**, 195428 (2008).
[11] H. Padmanabhan and B. R. K. Nanda, Phys. Rev. B **93**, 165403 (2016).
[12] Y. Jiang, P.-W. Lo, D. May, G. Li, G.-Y. Guo, F. B. Anders, T. Taniguchi, K. Watanabe, J. Mao, and E. Y. Andrei, Nat. Commun. **9**, 2349 (2018).
[13] M. V. Ulybyshev and M. I. Katsnelson, Phys. Rev. Lett. **114**, 246801 (2015).
[14] M. M. Ugeda, I. Brihuega, F. Guinea, and J. M. Gómez-Rodríguez, Phys. Rev. Lett. **104**, 096804 (2010).
[15] A. M. Valencia and M. J. Caldas, Phys. Rev. B **96**, 125431 (2017).
[16] V. Häfner, J. Schindler, N. Weik, T. Mayer, S. Balakrishnan, R. Narayanan, S. Bera, and F. Evers, Phys. Rev. Lett. **113**, 186802 (2014).
[17] N. M. R. Peres, F. Guinea, and A. H. Castro Neto, Phys. Rev. B **73**, 125411 (2006).

[18] N. Weik, J. Schindler, S. Bera, G. C. Solomon, and F. Evers, Phys. Rev. B **94**, 064204 (2016).

[19] A. V. Shytov, M. I. Katsnelson, and L. S. Levitov, Phys. Rev. Lett. **99**, 236801 (2007).

[20] A. V. Shytov, M. I. Katsnelson, and L. S. Levitov, Phys. Rev. Lett. **99**, 246802 (2007).

[21] V. M. Pereira, J. Nilsson, and A. H. Castro Neto, Phys. Rev. Lett. **99**, 166802 (2007).

[22] M. M. Fogler, D. S. Novikov, and B. I. Shklovskii, Phys. Rev. B **76**, 233402 (2007).

[23] R. R. Biswas, S. Sachdev, and D. T. Son, Phys. Rev. B **76**, 205122 (2007).

[24] E. B. Kolomeisky, J. P. Straley, and H. Zaidi, Phys. Rev. B **88**, 165428 (2013).

[25] D. P. DiVincenzo and E. J. Mele, Phys. Rev. B **29**, 1685 (1984).

[26] R. Jackiw and C. Rebbi, Phys. Rev. D **13**, 3398 (1976).

[27] A. J. Heeger, S. Kivelson, J. R. Schrieffer, and W. P. Su, Rev. Mod. Phys. **60**, 781 (1988).

[28] R. Jackiw and J. Schrieffer, Nucl. Phys. B **190**, 253 (1981).

[29] A. N. Redlich, Phys. Rev. Lett. **52**, 18 (1984).

[30] A. J. Niemi and G. W. Semenoff, Phys. Rev. Lett. **51**, 2077 (1983).

[31] A. J. Niemi and G. W. Semenoff, Phys. Rev. D **32**, 471 (1985).

[32] D. Boyanovsky and R. Blankenbecler, Phys. Rev. D **31**, 3234 (1985).

[33] R. Blankenbecler and D. Boyanovsky, Phys. Rev. D **31**, 2089 (1985).

[34] R. Blankenbecler and D. Boyanovsky, Phys. Rev. D **34**, 612 (1986).

[35] R. Jackiw, Phys. Rev. D **29**, 2375 (1984).

[36] T. Jaroszewicz, Phys. Rev. D **34**, 3128 (1986).

[37] C. R. Hagen, Phys. Rev. Lett. **64**, 503 (1990).

[38] G. W. Semenoff, Phys. Rev. Lett. **53**, 2449 (1984).

[39] F. D. M. Haldane, Phys. Rev. Lett. **61**, 2015 (1988).

[40] E. Fradkin, E. Dagotto, and D. Boyanovsky, Phys. Rev. Lett. **57**, 2967 (1986).

[41] C. Chamon, C.-Y. Hou, R. Jackiw, C. Mudry, S.-Y. Pi, and G. Semenoff, Phys. Rev. B **77**, 235431 (2008).

[42] R. Jackiw and G. Semenoff, Phys. Rev. Lett. **50**, 439 (1983).

[43] V. N. Kotov, B. Uchoa, V. M. Pereira, F. Guinea, and A. H. Castro Neto, Rev. Mod. Phys. **84**, 1067 (2012).

[44] D. C. Elias, R. V. Gorbachev, A. S. Mayorov, S. V. Morozov, A. A. Zhukov, P. Blake, L. A. Ponomarenko, I. V. Grigorieva, K. S. Novoselov, F. Guinea, and A. K. Geim, Nat. Phys. **7**, 701 (2011).

[45] See Supplemental Material at http://link.aps.org/supplemental/10.1103/PhysRevB.102.075109 for further discussion on the validity of the Dirac model, an explicit derivation of the formula for the charge density $\rho(\boldsymbol{r})$, an explicit derivation of the most general boundary condition associated with a nonpenetrable circular wall, an explicit derivation of the expression for and $\rho(\boldsymbol{r})$, details on our numerical calculations and the effects of boundary conditions, and an explicit calculation of the charge density $\rho(\boldsymbol{r})$ in the presence of multiple vacancies.

[46] M. Stone, Phys. Rev. B **31**, 6112 (1985).

[47] A. J. Niemi and G. W. Semenoff, Phys. Rev. D **30**, 809 (1984).

[48] C. Callias, Commun. Math. Phys. **62**, 213 (1978).

[49] In the presence of a defect, the Dirac points $K$ and $K'$ may be coupled, which is inconsistent with the single valley continuum Dirac equation. As shown in Ref. [59], for the case of a Gaussian scatterer with range $R = a$, the ratio between the intervalley and intravalley coupling is small (around $\sim$0.05). Thus, we neglect this coupling here, an assumption that will be further justified numerically .

[50] M. V. Berry and R. J. Mondragon, Proc. R. Soc. London, Ser. A **412**, 53 (1987).

[51] M. F. Atiyah, V. K. Patodi, and I. M. Singer, in *Mathematical Proceedings of the Cambridge Philosophical Society* (Cambridge University Press, Cambridge, 1975), Vol. 77, pp. 43–69.

[52] E. Akkermans and R. Narevich, Philos. Mag. B **77**, 1097 (1998).

[53] E. Akkermans, J. Avron, R. Narevich, and R. Seiler, Eur. Phys. J. B **1**, 117 (1998).

[54] There exists alternative choices of chiral boundary conditions, e.g., by projecting the zero modes onto a different angular momentum subspace. However, this would yield a zero mode decaying faster than $1/r$ and with a dimension-full strength.

[55] Note that it is not allowed to move the $\lim_{z\to 0}$ through the integral in (16).

[56] The sign of the Coulomb potential depends on $\operatorname{sign} M$ and whether the vacancy is from sublattice $T_A$ or $T_B$. The resulting spectrum remains unchanged in either case but will represent particle or hole states accordingly.

[57] Y. N. Demkov and V. N. Ostrovskii, *Zero-Range Potentials and their Applications in Atomic Physics* (Springer Science & Business Media, New York, 2013).

[58] P. J. Davis, *Interpolation and Approximation* (Dover publications, New York, 1975), pp. 268–269.

[59] T. Ando and T. Nakanishi, J. Phys. Soc. Jpn. **67**, 1704 (1998).